Journal of Pharmaceutical Analysis 12 (2022) 436–445

Contents lists available at ScienceDirect

Journal of Pharmaceutical Analysis

journal homepage: www.elsevier.com/locate/jpa

Original article

Nitrogen-doped carbon@TiO_2 double-shelled hollow spheres as an electrochemical sensor for simultaneous determination of dopamine and paracetamol in human serum and saliva

Hui Yang [a], Gongxun Cao [a], Yongjun Huang [a], Ye Lin [a], Fengying Zheng [a], Luxiu Lin [a, b, c], Fengjiao Liu [a, b, c], Shunxing Li [a, b, c, *]

[a] College of Chemistry, Chemical Engineering and Environment, Minnan Normal University, Zhangzhou, Fujian, 363000, China
[b] Fujian Provincial Key Laboratory of Pollution Monitoring and Control, Minnan Normal University, Zhangzhou, Fujian, 363000, China
[c] Fujian Key Laboratory of Separation and Analysis Science and Technology, Zhangzhou, Fujian, 363000, China

ARTICLE INFO

Article history:
Received 4 November 2020
Received in revised form
21 August 2021
Accepted 30 August 2021
Available online 1 September 2021

Keywords:
Electrochemical sensor
Simultaneous determination
Paracetamol
Dopamine

ABSTRACT

As the most commonly used antipyretic and analgesic drug, paracetamol (PA) coexists with neurotransmitter dopamine (DA) in real biological samples. Their simultaneous determination is extremely important for human health, but they also interfere with each other. In order to improve the conductivity, adsorption affinity, sensitivity, and selectivity of TiO_2-based electrochemical sensor, N-doped carbon@-TiO_2 double-shelled hollow sphere (H–C/N@TiO_2) is designed and synthesized by simple alcoholic and hydrothermal method, using polystyrene sphere (PS) as a template. Meanwhile, TiO_2 hollow spheres (H–TiO_2) or N-doped carbon hollow spheres (H–C/N) are also prepared by the same method. H–C/N@TiO_2 has good conductivity, charge separation, and the highly enhanced and stable current responses for the detection of PA and DA. The detection limit and linear range are 50.0 nmol/L and 0.3–50 μmol/L for PA, 40.0 nmol/L and 0.3–50 μmol/L for DA, respectively, which are better than those of carbon-based sensors. Moreover, this electrochemical sensor, with high selectivity, strong anti-interference, high reliability, and long time durability, can be used for the simultaneous detection of PA and DA in human blood serum and saliva. The high electrochemical performance of H–C/N@TiO_2 is attributed to the multifunctional combination of different layers, because of good conductivity, absorption and electrons transfer ability from in-situ N-doped carbon and electrocatalytic activity from TiO_2.

1. Introduction

Paracetamol (PA, $C_8H_9NO_2$), one of the most commonly used antipyretic and analgesic drugs, is known as acetaminophen [1]. It can usually be used to treat pain, headache, fever, migraines, arthritis, postoperative pain, etc. [2–4], but its human resistance is 50 mg/L. The overdose of PA causes severe liver damage and high accumulation of toxic metabolites, which can be fatally hepatotoxic [5,6] and nephrotoxic [4,7]. Dopamine (DA, $C_8H_{12}O_2N$) plays an important role in human body, when the lack of DA leads to a variety of diseases including Parkinson's disease and schizophrenia [8–11]. Moreover, the detection of them can be affected by their coexistence [12]. It is extremely important for us to protect human health from some dangerous diseases by the simultaneous determination of PA and DA. Many analytical methods that have been developed to detect DA and PA include titrimetry, UV–vis spectrophotometry, capillary electrophoresis, high performance liquid chromatography, and chemiluminescence [13–19], but there are some disadvantages in these methods, including time-consuming, tedious sample pretreatment processes, and high cost. Due to the advantages of electrochemical techniques (e.g., selectivity, sensitivity, low cost, simple instrumentation, facile miniaturization, and rapid response), it is essential for us to establish an electrochemical sensor for simultaneous, rapid, simple, accurate, and sensitive determination of PA and DA.

As an increasingly popular photocatalyst, sensor, UV absorber, and energy storage, the properties of TiO_2 are low cost, non-

Peer review under responsibility of Xi'an Jiaotong University.

* Corresponding author. College of Chemistry, Chemical Engineering and Environment, Minnan Normal University, Zhangzhou, Fujian, 363000, China.
E-mail address: lishunxing@mnnu.edu.cn (S. Li).

https://doi.org/10.1016/j.jpha.2021.08.005

toxicity, semi-conductivity, thermal and chemical stability, excellent biocompatibility and high uniformity [20–23]. Its application as an electrochemical sensor is limited by its low conductivity, high recombination rate of photo-generated electrons and holes [24,25], and poor affinity with organic compounds (e.g., PA and DA). To overcome these shortcomings, TiO_2 is combined with carbon nanotube or graphene carbon, but this combination still cannot meet our requirements. Heteroatom (e.g., N, B, S) doping can improve the electrochemical performance of carbon. Synergistic effect of heteroatom can effectively compensate for the disadvantages of carbon materials because the lone electron pairs from heteroatoms can supply additional negative charges to carbon networks [26–29]. In addition, the structures of TiO_2-based nanomaterials have significant effects on their catalytic activities, and double-shelled hollow spheres bring more heterojunctions interfaces and multi-active sites [30,31]. Hence, N-doped carbon@TiO_2 double-shelled hollow sphere (H–C/N@TiO_2) is adopted as an electrochemical sensor for detection of PA and DA with the advantages as follows. First, the synthesis process is simple, less dangerous, less time consuming, and environmentally friendly. Second, it is essential for specific electrochemical reactions. Third, the synergistic effect of N-doped carbon and TiO_2 can be utilized, including electrocatalysis and edge-plane defect sites. The joint of N-doped carbon and TiO_2, including TiO_2 nanoparticles@N-doped carbon [32], core-shell mesoporous N-doped carbon@TiO_2 [33], N-doped carbon sheets@TiO_2 nanoparticles [34], and N-doped carbon tuning yolk-like TiO_2 [35], have been developed for the degradation of organic pollutants [32], lithium-ion and sodium-ion batteries [33,35], glucose determination [34], and oxygen reduction and evolution [32–36]. To date, H–C/N@TiO_2 as an electrochemical sensor for the detection of PA and DA has not been reported.

Herein, a green and novel method for in situ H–C/N@TiO_2 is proposed by us. As a hard template, the surface functionalization of polystyrene microspheres (PSs) is adopted because size-controlled monodisperse (TiO_2@PS) can be prepared. And then a layer of nitrogen-rich carbons, with abundant functional groups (including C–O, –OH, and N–H) and reduction ability, is wrapped onto TiO_2@PS. After calcination, H–C/N@TiO_2 is obtained. Ultimately, H–C/N@TiO_2 is modified onto a glassy carbon electrode (GCE) as an electrochemical sensor, which can simultaneously, sensitively, and selectively detect PA and DA in human serum and saliva.

2. Experimental

All reagents and apparatus are shown in Supplementary data.

2.1. Synthesis of TiO_2 hollow spheres

According to the literature [37,38], PSs with an average diameter of about 250 nm were synthesized as support information (SI1). Ultra-pure water (0.15 mL), ethanol (72 mL), polyethylene pyrrolidone (K30, 0.01 g), and PS (1 mL) were added into a round bottom flask (150 mL) for sonication of 10 min. N-tetrabutyl titanate (0.18 mL) was also added into the above solution, heated to 80 °C, and refluxed for 4 h. The resultant microspheres (TiO_2@PS) were rinsed three times with ethanol and dried at 60 °C under vacuum for 6 h. Ultimately, they were heated to 550 °C with a rate of 5 °C/min and calcined for 3 h in a muffle furnace. PSs were removed and the products, TiO_2 hollow spheres (H–TiO_2, 550 °C), were synthesized.

2.2. Synthesis of H–C/N@TiO_2 double-shelled hollow spheres and H–TiO_2, H–C/N hollow spheres

After dispersing of hollow spheres (H–TiO_2, 550 °C, 60 mg) in Tris-HCl (100 mL, 10 mmol/L, pH 8.5) solution, DA (50 mg) was added and stirred for 24 h at room temperature. The products (Polydopamine (PDA) @TiO_2) were rinsed three times with ultra-pure water and dried at 60 °C under vacuum for 24 h. The PDA@TiO_2 hollow spheres were heated to 800 °C with a rate of 5 °C/min and calcined at 800 °C for 2 h in a tubular atmosphere furnace (under N_2 protection). The products (H–C/N@TiO_2) were synthesized. Moreover, H–C/N was prepared by the same method.

2.3. Preparation of modified glass carbon electrodes (GCE)

The bare GCE was pretreated as follows, including polishing until to a mirror-finish successively with 1 μm, 0.3 μm, and 0.05 μm of alumina slurry, washed with anhydrous ethanol and

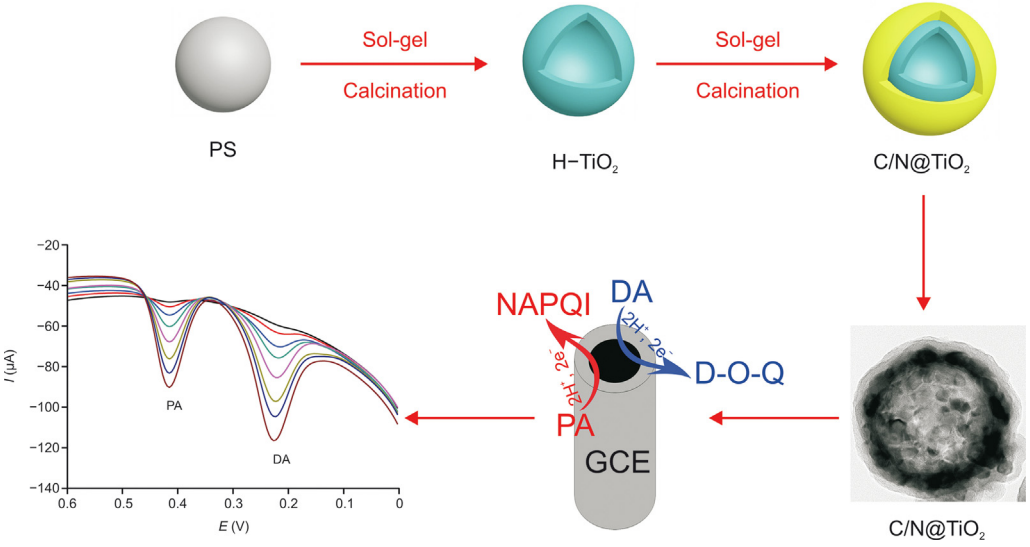

Scheme 1. Schematic diagrams of 3-dimensional nitrogen-doped carbon@TiO_2 double-shelled hollow sphere synthesis and electrochemical sensing.

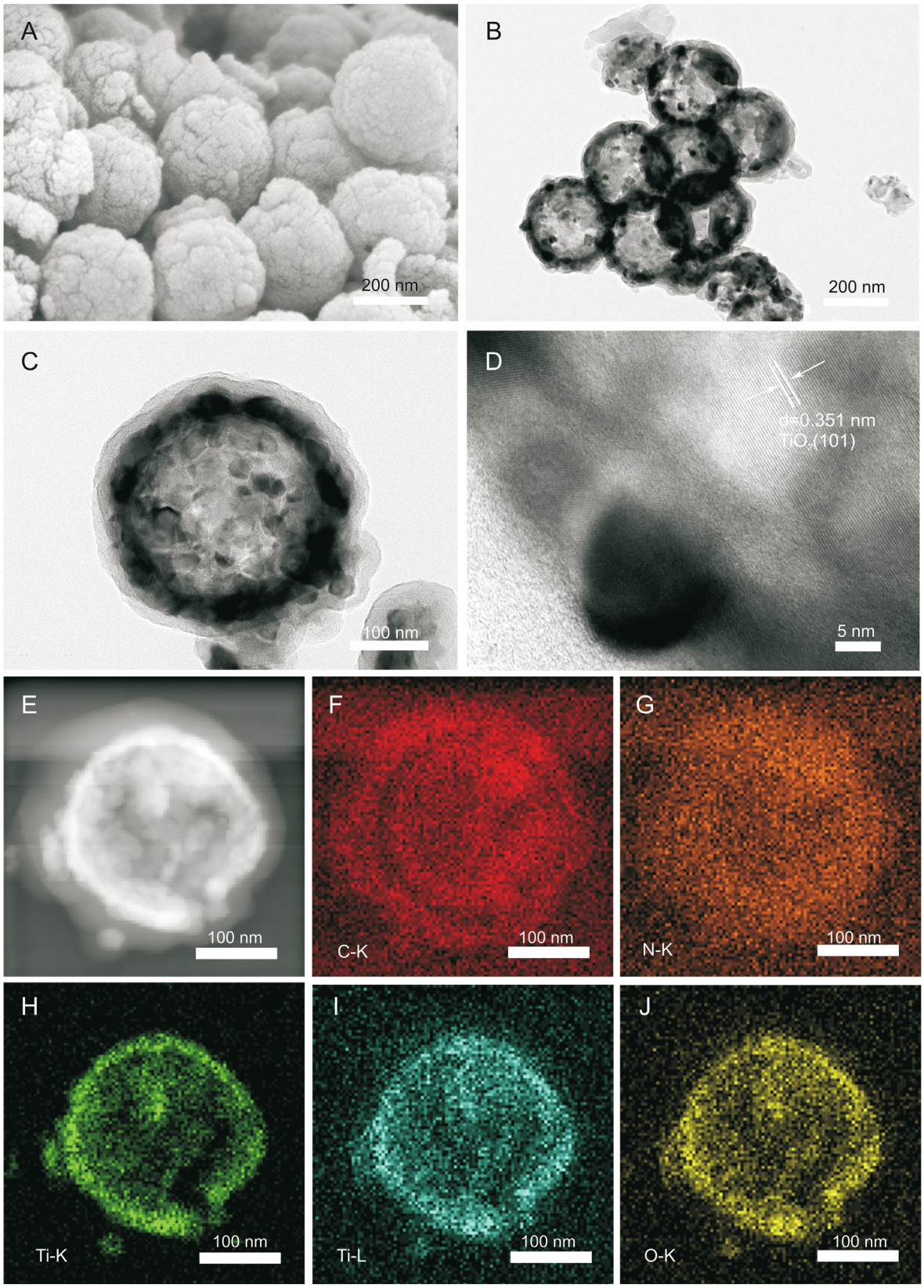

Fig. 1. (A) Scanning electron microscopy (SEM) images of H–C/N@TiO_2. (B–D) Transmission electron microscopy (TEM) images of H–C/N@TiO_2. (E–J) High angle annular dark field-scanning transmission electron microscopy (HAADF-STEM) mapping images of H–C/N@TiO_2.

water in an ultrasonic bath successively, and then dried by N_2 blowing. H–C/N@TiO_2 (or H–TiO_2, or H–C/N, 2 mg) was dispersed in 200 μL of mixture solution (including 20 μL of chitosan solution and 180 μL of water). Then, the above-prepared solution (1 mg/mL, 5 μL) was cast onto the surface of pretreated bare GCE and dried at room temperature. These electrodes were

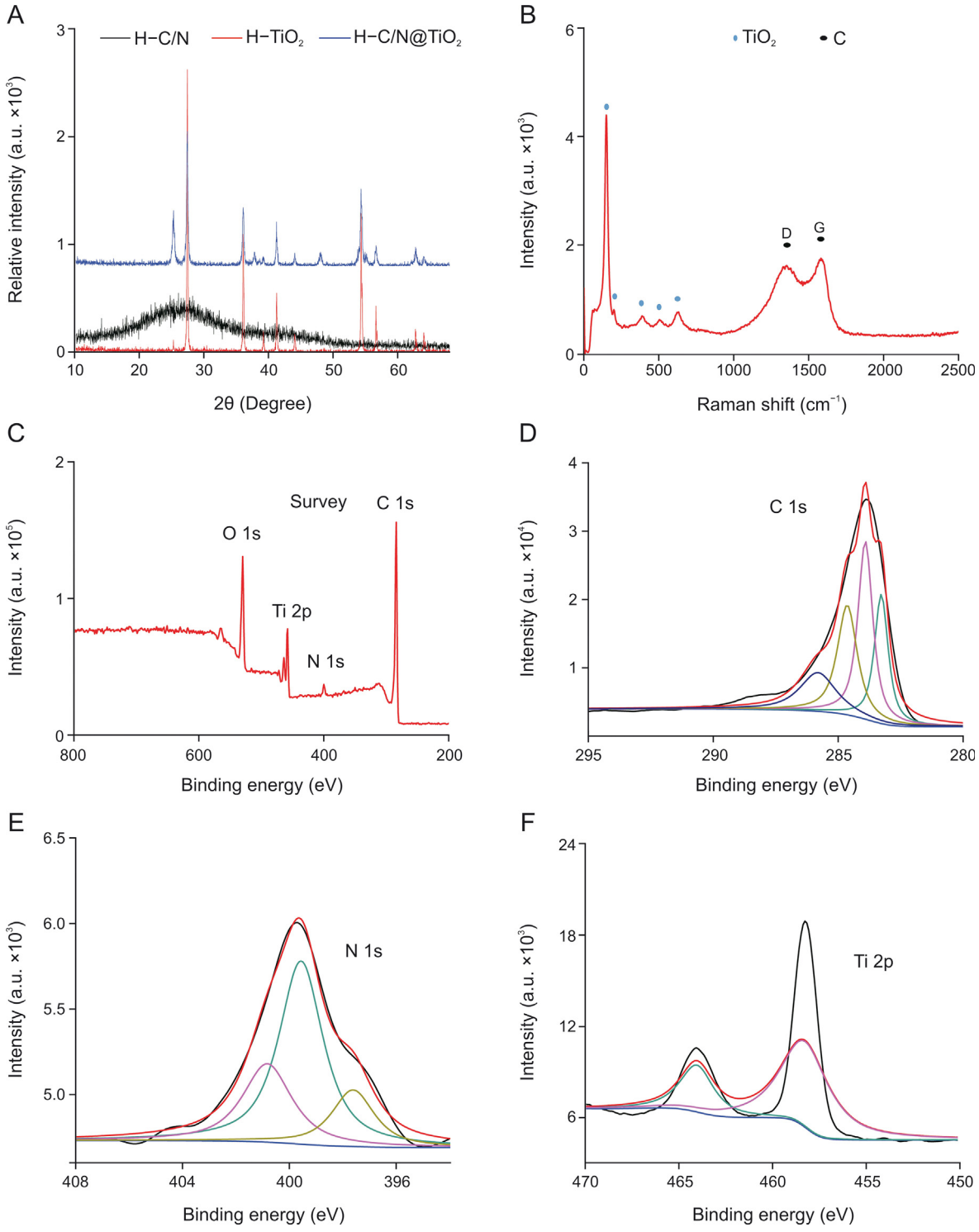

Fig. 2. (A) X-ray diffraction (XRD) patterns of the as-synthesized H–C/N, H–TiO_2, and H–C/N@TiO_2. (B) Raman spectra of H–C/N@TiO_2. (C) X-ray photoelectron spectroscopy (XPS) survey spectra of H–C/N@TiO_2 in the range of 200–800 eV. (D–F) X-ray photoelectron spectroscopy (XPS) of C 1s, N 1s, and Ti 2p from H–C/N@TiO_2.

noted as H–C/N@TiO_2/GCE, H–C/N/GCE, and H–TiO_2/GCE, respectively.

2.4. Electrochemical measurements

Electrochemical measurements with differential pulse voltammetry (DPV) were performed by an Electrochemical Workstation (CHI 660E, Chenhua Instrument Co., Shanghai, China) with a three-electrode system and conducted from 0.0 to 0.6 V at room temperature with a pulse amplitude of 100 mV/s in 0.1 mol/L of phosphate buffer solution (PBS). The modified GCE (H–C/N@TiO_2/GCE, H–C/N/GCE, or H–TiO_2/GCE), platinum wire, and Ag/AgCl/saturated KCl were used as the working, counter, and reference electrodes, respectively.

3. Results and discussion

3.1. Synthesis and characterization of H–C/N@TiO_2

In this study, the synthetic methods, including self-adsorption/reduction, simple template method, and carbonization, were used to construct 3D freestanding H–C/N@TiO_2 as shown in Scheme 1. During the self-polymerization for the preparation of TiO_2@PS, the solution color was white and never changed. Then TiO_2@PS was calcined. During the preparation of PDA@TiO_2, the color of solution was changed from white to black. H–TiO_2 served as not only a hollow ball template but also an adsorption agent for PDA during the preparation of PDA@TiO_2.

Scanning electron microscopy (SEM) was used to characterize the morphologies of H–C/N@TiO_2 as shown in Fig. 1A. It can be clearly seen that the products were hollow and exhibited high monodispersity and uniform size, revealing that PDA shell could be wrapped uniformly onto H–TiO_2. The SEM images of H–TiO_2 and H–C/N are shown in Fig. S1. The transmission electron microscopy (TEM) images of these nanocomposites confirmed that the produces were hollow (Fig. 1B), which were consistent with the results of SEM. H–C/N@TiO_2 with uniform thick and clearly layered shell is shown in Fig. 1C. Besides, the high resolution transmission electron microscopy (HRTEM) image of H–C/N@TiO_2 showed that the lattice spacing of 0.351 nm corresponded to the (101) plane of TiO_2 (Fig. 1D). To further indicate the distribution of elements, high angle annular dark field-scanning transmission electron microscopy (HAADF-STEM) was used for the characterization of H–C/N@TiO_2. The HAADF-STEM mapping images are shown in Figs. 1E–J, indicating that C, N, Ti, and O were uniformly enriched on the surface of the hollow sphere. The red, orange-red, green, blue-green, and yellow colored areas in HAADF-STEM mapping images (Figs. 1F–J) revealed that H–C/N@TiO_2 was the combination of C, N, Ti, and O, respectively. Moreover, it could also be seen that the distribution of Ti and C was a hierarchical structure from the elemental images of H–C/N@TiO_2. X-ray diffraction (XRD) was used for the characterization of H–C/N@TiO_2, H–C/N, and H–TiO_2. As shown in Fig. 2A, the diffraction peaks at 25.3°, 37.7°, 47.9°, 53.8°, and 62.6° could correspond to (101), (004), (200), (105), and (204) reflection of anatase TiO_2, respectively. While the peaks at 27.8°, 35.9°, 41.30°, 44.10°, 56.69°, and 64.09° could be specified as (110), (101), (111), (210), (220), and (310) from the reflection of rutile TiO_2, respectively. The diffraction peaks at 26.1° and 43° corresponded to (102) and (100) reflection of graphite carbon. In addition, two characteristic peaks of graphitized carbon (about 1347 and 1583 cm^{-1}) and the characteristic peaks of TiO_2 (about 144, 200, 397, 516, and 639 cm^{-1}) were also observed in the Raman spectrum of H–C/N@TiO_2 as shown in Fig. 2B. These characterizations revealed that in situ H–C/N@TiO_2 could be constructed successfully. In addition, the chemical bonding and elemental composition of the H–C/N@TiO_2 composite were also further measured by X-ray photoelectron spectroscopy (XPS) in the range of 200–800 eV. The XPS spectra of H–C/N@TiO_2 (Fig. 2C) indicated the coexistence of Ti, C, N, and O in nanomaterials. Four different constituent peaks (C=C, C–N, C–O–C, and C=O) were observed in the spectrum of C 1s (Fig. 2D) at 283.6, 284.3, 286.4, and 288.1 eV, respectively. High-resolution XPS N 1s spectra (Fig. 2E) of the as-prepared composites were determined as the types of nitrogen dopants. In the high-resolution XPS N 1s spectrum, three types of nitrogen (pyridinic, pyrrolic and graphitic N) were observed and the constituent peaks corresponded to 397.5, 400.1 and 401.9 eV, respectively. The content of pyrrolic N was the highest among three types of nitrogen dopants in composites, indicating that there would be abundant adsorption sites for organic contaminants [39]. As shown in Fig. 2F, the constituent peaks of Ti 2p3/2 and Ti 2p1/2 corresponded to 458.2 and 464.2 eV in the high resolution XPS Ti 2p spectrum. As an electrode material, it would provide more absorption sites for analytical targets with N, offer a good conductivity by C, and high electrocatalysis performance by TiO_2. The above-mentioned advantages as an electrochemical sensor were tested by the identification and detection of PA and DA in human serum and saliva.

3.2. Electrochemical behavior of H–C/N@TiO_2 composites

In the electrochemical experimental section, the electrochemical properties of different electrodes, including GCE, H–C/N/GCE, H–TiO_2/GCE, and H–C/N@TiO_2/GCE, were tested by cyclic voltammetry (CV), using 0.1 mol/L of PBS (pH 6.0, containing 50 μmol/L of PA and DA). As shown in Fig. 3, the redox peaks of PA and DA for H–C/N@TiO_2/GCE were the clearest in them and could be used for qualitative and quantitative analyses of DA and PA. Moreover, the DPV of the samples is also provided as Fig. S2. H–C/N@TiO_2 was obviously superior to the others because it not only had the good conductivity of C but also had the superior redox of TiO_2. The order of Ret values as GCE > H–TiO_2/GCE > H–C/N/GCE > H–C/N@TiO_2/GCE can be gained from Fig. 3. In addition, two pairs of significant redox peaks belonged to PA and DA, which further revealed the importance of the construct of double-shell in electroanalysis.

3.3. Effect of scan rate and pH

To demonstrate the transport characteristics of H–C/N@TiO_2/GCE, the relationship of the redox peak currents of PA and DA with the scan rate was studied in the range of 20–400 mV/s, which is shown in Figs. 4A and B. The linear regression equations for PA were $I_{pc}(\mu A) = 12.237 + 0.2170\,v$ ($R^2 = 0.9976$), $I_{pa}(\mu A) = -31.503 - 0.3399\,v$ ($R^2 = 0.9954$), and the DA linear regression equations were $I_{pc}(\mu A) = 11.336 + 0.3834\,v$ ($R^2 = 0.9972$), $I_{pa}(\mu A) = -29.161 - 0.5874\,v$ ($R^2 = 0.9968$). According to these results, the electro-redox reaction of DA and PA was a typical adsorption-controlled process. The linear of the plots of log *I*p versus log *v* in the scan rate with slopes of 0.783 for DA and 0.656 for PA, respectively, are shown in Fig. S3, and then the adsorption-controlled process of DA and PA could be confirmed further.

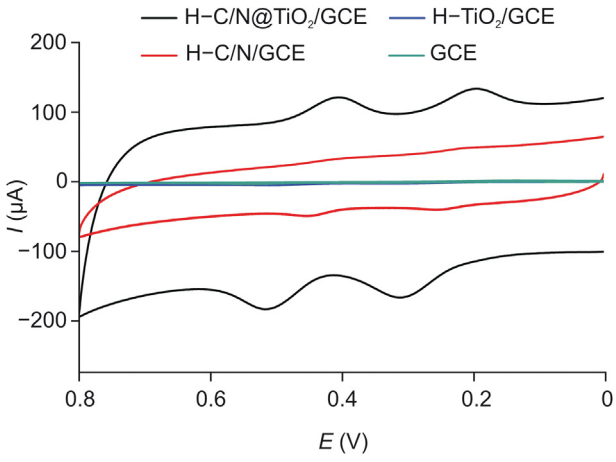

Fig. 3. Cyclic voltammetry of the different electrodes in 0.1 mol/L of PBS (pH 6.0, containing 50 μmol/L of PA and DA), at scan rate of 100 mV/s.

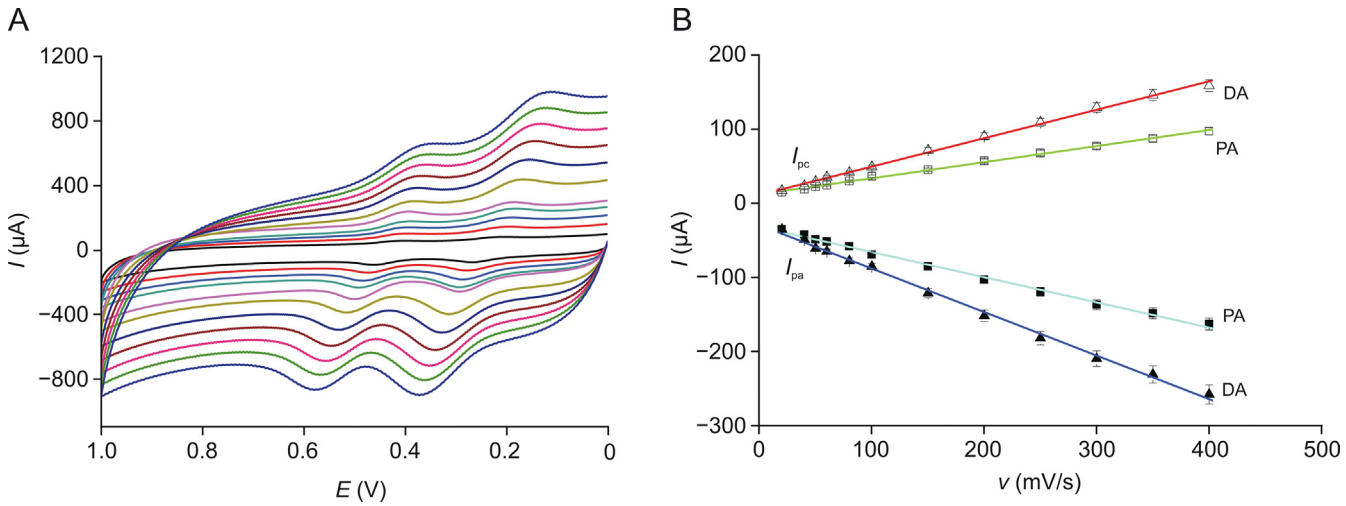

Fig. 4. (A) Cyclic voltammetry of GCE modified by H–C/N@TiO_2 at different scan rates in 0.1 mol/L of PBS (pH 6.0, containing 50 μmol/L of PA and DA). (B) Curve of redox peak current vs. scan rate for PA and DA.

The redox peak currents of PA and DA in the range of 0.8 −0.0 V were influenced by the pH of the electrolyte (50 μmol/L of PA and DA, in 0.1 mol/L of PBS), as shown in Fig. S4. It was beneficial to estimating the ratio of proton to electron in this reaction. As shown in Fig. 5A, the redox peak current value was the maximum response when the pH value of PBS was 6.0. Therefore, pH of the solution was determined at 6.0 in the following experiments. The linear relationship between the peak potentials and pH of the solution with E_{PA} = 0.8770−0.0634 pH (R^2 = 0.9815), E_{DA} = 0.6613−0.0629 pH (R^2 = 0.9880) is shown in Fig. 5B. According to the formula (d*E*p/dpH=2.303 mRT/nF, where m and n are the numbers of proton and electron, respectively), the slopes of the two regression equations, 0.0634 and 0.0629 for PA and DA, approached the theoretical value [40,41], indicating that the electrochemical redox of PA and DA on the electrode of H–C/N@TiO_2/GCE should be a two-electron and two-proton process.

3.4. Qualitative and quantitative determination of PA and DA

The DPV measurements for qualitative and quantitative analyses were better than those of CV technique in respect of sensitivity and resolution because a small voltage pulse superimposed on the linear voltage sweep was applied and the differential current at a short time after the pulse was sampled by DPV. Hence, DPV was used to assess the quantitative and qualitative analyses of PA and DA. As shown in Fig. 6A and B, the redox peaks currents of PA or DA at H–C/N@TiO_2/GCE increased gradually with the concentration increase and a good linear relationship was established. As the concentration of PA increased, two linearities were observed with two linear regression equations, i.e., I_{pa} = −4.8417−3.2596*c* (R^2 = 0.9910) for 0.3–20 μmol/L, I_{pa} = −48.1253−0.9894*c* (R^2 = 0.9964) for 20–50 μmol/L in Fig. 6D. The linearity for DA was increased from 0.3 to 50 μmol/L with linear regression equation of I_{pa} = −5.9062−2.0480*c* (R^2 = 0.9934) in Fig. 6E.

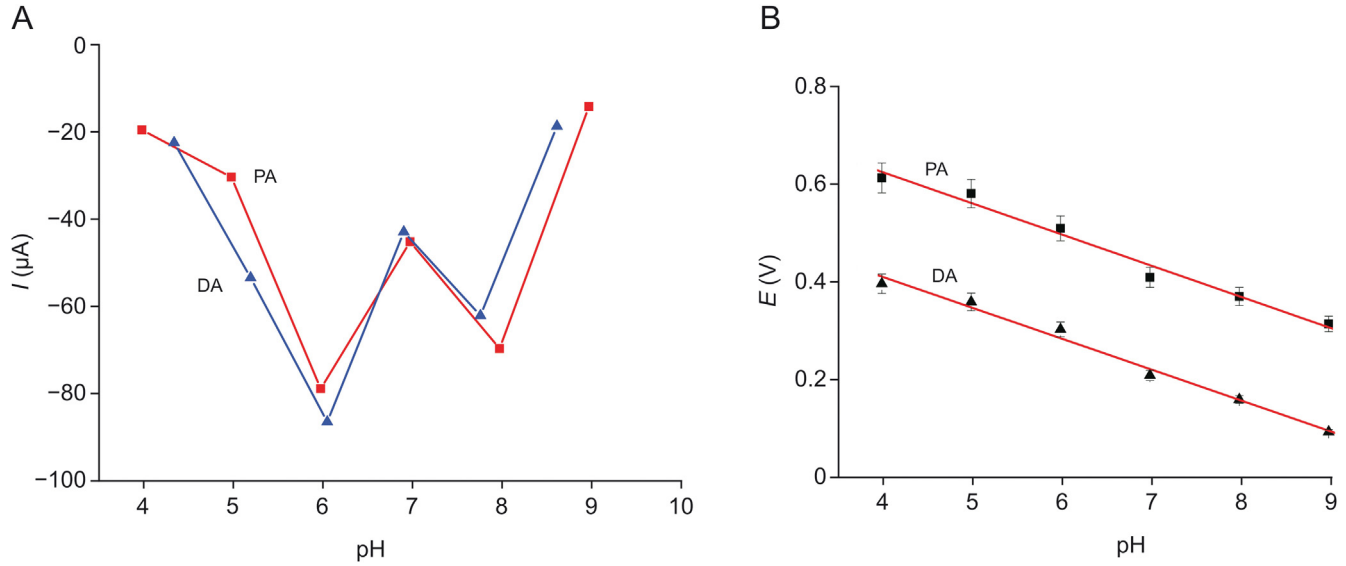

Fig. 5. Electrochemical behavior of H–C/N@TiO_2 in 0.1 mol/L of PBS (containing 50 μmol/L of PA and DA) with different pH values. Relationship between (A) peak current, (B) peak potential and pH.

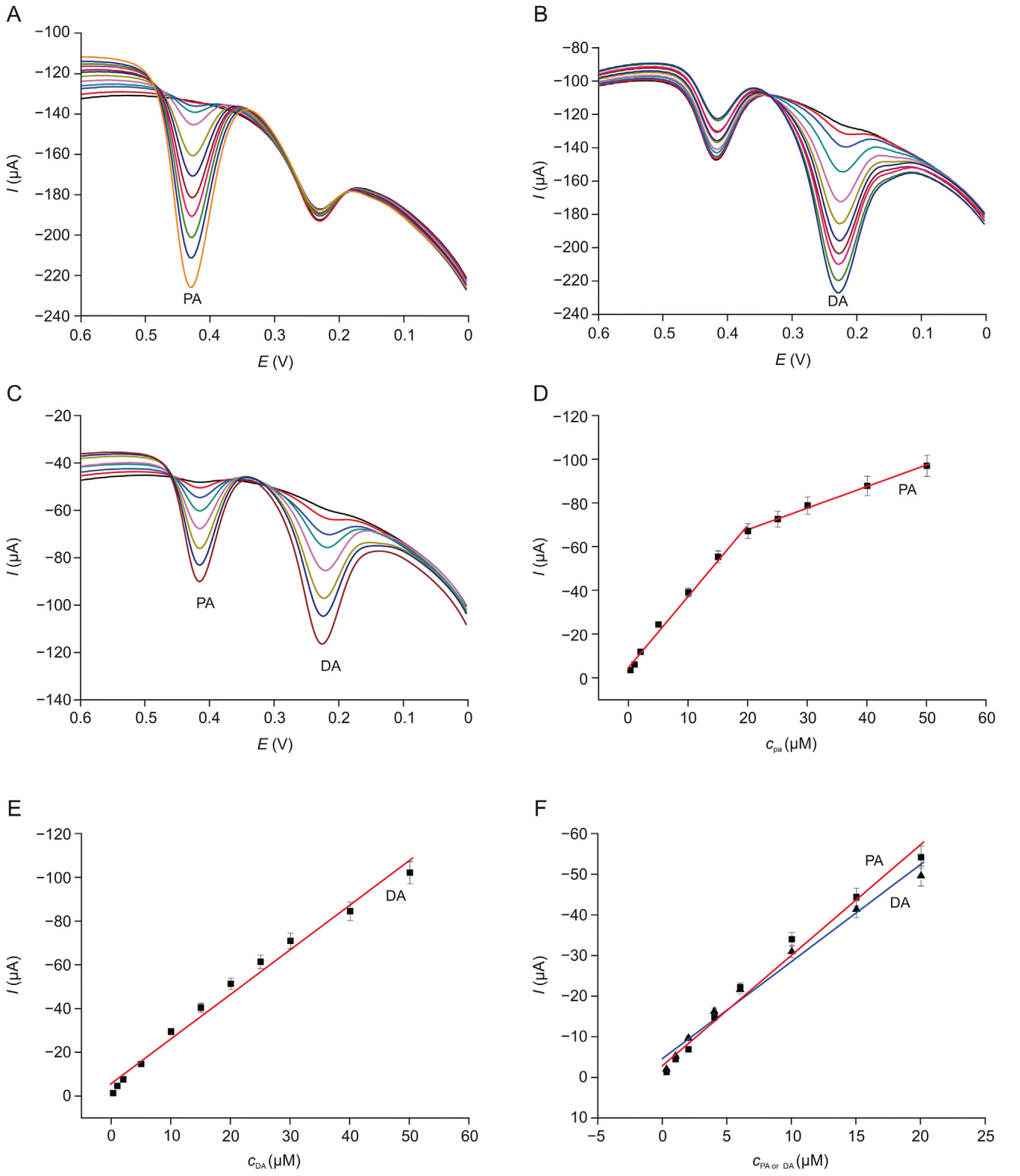

Fig. 6. Differential pulse voltammetry (DPV) for (A) PA, (B) DA and (C) both mixture in 0.1 mol/L of PBS (pH 6.0) with H–C/N@TiO_2/GCE, at scan rate of 100 mV/s. Calibration plots of oxidation current vs. (D) PA, (E) DA, and (F) both mixture concentrations. DPV curves increment: 0.004 V, amplitude: 0.05 V, pulse width: 0.05 s, sampling width: 0.0167 s, pulse period: 0.5 s, quiet time: 2 s.

According to the signal-to-noise ratio (S/N = 3), the detection limit was estimated to be 50 and 40 nmol/L for PA and DA, respectively. Analytical performance (including linear range and limit of detection) of the other materials was compared and is shown in Table 1 [12,42–49], which revealed that the detection limit of our work was the best. Hence, the superior performance of H–C/N@TiO_2/GCE showed a promising platform for the simultaneous electrochemical determination of DA and PA.

Table 1
Analytical performance of electrodes for determination of PA and DA by differential pulse voltammetry (DPV).

Electrodes	Linear range (μmol/L)		Detection limit (μmol/L)		Refs.
	DA	PA	DA	PA	
Cu/Cu_2O-OA/MWCNTs/GC	0.02–0.159	1–142.9	0.00327	1.51	[12]
MWCNT-BPVCM-e/GCE	5–1000	5–1000	2.3	3.5	[42]
f-MWCNT/GCE	3–200	3–300	0.8	0.6	[43]
PAY/nano-TiO_2/GC	–	12–120	1.0	2.0	[44]
MWCNT/CCE	0.05–320	0.1–320	0.22	0.12	[45]
ZIF-67/GCE	2–45	2–45	1.3	1.4	[46]
NiO–CuO/GR/GCE	0.5–20	4–400	0.17	1.33	[47]
GI/GCE	NA	10–500	NA	2.7	[48]
$CoFe_2O_4$	3–180	3–200	0.35	0.25	[49]
H–C/N@TiO_2/GCE	0.3–50	0.3–50	0.040	0.050	This wok

In addition, the simultaneous analysis of DA and PA was further carried out by DPV. As shown in Figs. 6C and F, when the concentrations of DA and PA increased from 0.3 to 20 μmol/L at H–C/N@TiO_2/GCE, the redox peak currents also increased proportionally with two linear regression equations of $I_{pa} = -4.7308-2.3984c_{PA}$ ($R^2 = 0.9805$), $I_{pa} = -3.0063-2.285c_{DA}$ ($R^2 = 0.9835$), and the linear correlation coefficients were 0.9805 and 0.9835 for PA and DA, respectively. These results indicated that H–C/N@TiO_2/GCE could be applied to identify and determinate DA and PA simultaneously as an electrochemical sensor.

In order to assess the selectivity of H–C/N@TiO_2/GCE, the electrolyte coexisted with ions and organic substances (including sodium chloride, potassium chloride, sodium acetate, and glucose, 10 μmol/L) in PBS (0.1 mol/L, pH 6.0, with 1 μmol/L of PA and DA) and was then simultaneously determined by DPV. The results showed current variation was less than 5% after adding interfering substances, indicating that this nanomaterial as an electrochemical sensor had a strong anti-interference ability for analysis of PA and DA. In addition, PA and DA were determined every 3 days and its redox activity could be kept for nearly 15 days. The stability of the H–C/N@TiO_2/GCE was evaluated by repeating five measurements in the same solution containing 1 μmol/L of DA and PA. A relative standard deviation (RSD) of 1.78% was obtained for five successive measurements, which indicated that the sensor was not subjected to surface fouling by the oxidation products. So, experimental results revealed that the selectivity and repeatability of H–C/N@TiO_2/GCE were good for the simultaneous analysis of PA and DA.

To evaluate the feasibility of the sensor (H–C/N@TiO_2/GCE), the selective analysis of DA and PA was highly necessary in human serum and saliva. Human blood was collected from the City Hospital in Zhangzhou, Fujian, China, centrifuged, and stored at 4 °C in a refrigerator. Saliva samples were prepared according to the references [50,51]. They were diluted to 50 fold by 0.1 mol/L of PBS. Then the concentrations of DA and PA were determined by H–C/N@TiO_2/GCE. The results are shown in Table 2. The recoveries of DA and PA were 98.6%–102.4% and 101.4%–103.7%, respectively. These results proved that the influence of sample matrix on the determination of PA and DA could be overlooked. Hence, the sensor H–C/N@TiO_2/GCE could be used to identify and detect DA and PA simultaneously in human serum or saliva.

Table 2
Detection of PA and DA in real sample (human serum or saliva) using H–C/N@TiO_2/GCE.

Sample	Adding standard (μmol/L)		Detection level (μmol/L)		Recovery (%)	
	PA	DA	PA	DA	PA	DA
Saliva	0	0	ND	ND	0	0
	1	1	1.014	0.992	101.4	99.2
	2.0	1.5	2.039	1.515	102.0	101.0
Human serum	0	0	ND	ND	0	0
	1	1	1.031	0.986	103.1	98.6
	2.0	1.5	2.073	1.536	103.7	102.4

4. Conclusions

In this work, a high-performance electrochemical sensor for the identification and detection of PA and DA, in-situ H–C/N@TiO_2 was constructed, with a high conductivity, superior electrocatalytic performance, and reliable qualitative and quantitative capabilities. More importantly, the performance of electrocatalytic activity was excellent and the preparation of electrode materials was environmental friendly, with in-situ doping reaction and hard template method. Both excellent sensing linear range and sensitive detection limit for PA (0.3–50 μmol/L and 50 nmol/L) and DA (0.3–50 μmol/L and 40 nmol/L) could be offered by our sensor. A high-efficacy and economical analytical platform was proposed by us, used for ultrasensitive and highly selective detection of PA and DA from human serum or saliva. These satisfactory results were due to the synergistic effect of different components of TiO_2 and N-doped carbon with abundant functional groups (including C–O, –OH, and N–H) and reduction ability, the advantages of double-shelled hollow spheres.

CRediT author statement

Hui Yang: Conceptualization, Methodology, Investigation, Writing - Original draft preparation, Formal analysis, Data curation; **Gongxun Cao:** Investigation, Data curation; **Yongjun Huang:** Data curation; **Ye Lin:** Investigation; **Fengying Zheng:** Funding acquisition, Supervision; **Luxiu Lin:** Data curation; **Fengjiao Liu:** Data curation; **Shunxing Li:** Methodology, Funding acquisition, Writing - Reviewing and Editing, Supervision.

Declaration of competing interest

The authors declare that there are no conflicts of interest.

Acknowledgments

This work was supported by the National Natural Science Foundation of China (Grant Nos.: 22074058 and 21675077), the

Project of Industry-University-Research Cooperation of Fujian Province (Grant No.: 2019Y4010), and the Education-Science Research Project for Young and Middle-aged Teachers of Fujian (Grant No.: JAT200317).

Appendix A. Supplementary data

Supplementary data to this article can be found online at https://doi.org/10.1016/j.jpha.2021.08.005.

References

[1] Y.C. Li, S.Q. Feng, Y.M. Zhong, et al., Simultaneous and highly sensitive determination of hydroquinone and catechol using carboxyl functionalized graphene self-assembled monolayers, Electroanalysis 27 (2015) 2221–2229.
[2] T. Madrakian, E. Haghshenas, A. Afkhami, Simultaneous determination of tyrosine, acetaminophen and ascorbic acid using gold nanoparticles/multi-walled carbon nanotube/glassy carbon electrode by differential pulse voltammetric method, Sens. Actuators B chem. 193 (2014) 451–460.
[3] S. Wang, F. Xie, R. Hu, Carbon-coated nickel magnetic nanoparticles modified electrodes as a sensor for determination of acetaminophen, Sens. Actuators B Chem. 123 (2007) 495–500.
[4] E. Murugan, K. Kumar, Fabrication of SnS/TiO_2@GO composite coated glassy carbon electrode for concomitant determination of paracetamol, tryptophan, and caffeine in pharmaceutical formulations, Anal. Chem. 91 (2019) 5667–5676.
[5] B.G. Mahmoud, M. Khairy, F.A. Rashwan, et al., Simultaneous voltammetric determination of acetaminophen and isoniazid (hepatotoxicity-related drugs) utilizing bismuth oxide nanorod modified screen-printed electrochemical sensing platforms, Anal. Chem. 89 (2017) 2170–2178.
[6] M.T. Olaleye, B.T.J. Rocha, Acetaminophen-induced liver damage in mice: Effects of some medicinal plants on the oxidative defense system, Exp. Toxicol. Pathol. 59 (2008) 319–327.
[7] M. Mazer, J. Perrone, Acetaminophen-induced nephrotoxicity: Pathophysiology, clinical manifestations, and management, J. Med. Toxicol. 4 (2008) 2–6.
[8] D. Shankaran, K. Iimura, T. Kato, Simultaneous determination of ascorbic acid and dopamine at a sol-gel composite electrode, Sens. Actuators B Chem. 94 (2003) 73–80.
[9] V.V. Dutt, H.A. Mottola, Determination of uric acid at the microgram level by a kinetic procedure based on a “pseudo-induction” period, Anal. Chem. 46 (1974) 1777–1781.
[10] J. Njagi, M.M. Chernov, J.C. Leiter, et al., Amperometric detection of dopamine in vivo with an enzyme based carbon fiber microbiosensor, Anal. Chem. 82 (2010) 989–996.
[11] T. Iranmanesh, M.M. Foroughi, S. Jahani, et al., Green and facile microwave solvent-free synthesis of CeO_2 nanoparticle-decorated CNTs as a quadruplet electrochemical platform for ultrasensitive and simultaneous detection of ascorbic acid, dopamine, uric acid and acetaminophen, Talanta 207 (2020), 120318.
[12] M. Devaraj, R. Saravanan, R. Deivasigamani, et al., Fabrication of novel shape Cu and Cu/Cu_2O nanoparticles modified electrode for the determination of dopamine and paracetamol, J. Mol. Liq. 221 (2016) 930–941.
[13] R. Săndulescu, S. Mirel, R. Oprean, The development of spectrophotometric and electroanalytical methods for ascorbic acid and acetaminophen and their applications in the analysis of effervescent dosage forms, J. Pharm. Biomed. Anal. 23 (2000) 77–87.
[14] A. Safavi, M.A. Karimi, M.R.H. Nezhad, et al., Sensitive indirect spectrophotometric determination of isoniazid, Spectrochim. Acta A Mol. Biomol. Spectrosc. 60 (2004) 765–769.
[15] H.H. Liu, M.P. Li, R.B. Kaner, et al., Monolithically integrated self-charging power pack consisting of a silicon nanowire array/conductive polymer hybrid solar cell and a laser-scribed graphene supercapacitor, ACS Appl. Mater. Interfaces 10 (2018) 15609–15615.
[16] H.L. Yan, Y.P. Zhou, Q.J. Xie, et al., Simultaneous analysis of isoniazid and rifampicin by high-performance liquid chromatography with gradient elution and wall-jet/thin-layer electrochemical detection, Anal. Methods 6 (2014) 1530–1537.
[17] B. Wu, Z. Wang, Z. Xue, et al., A novel molecularly imprinted electrochemiluminescence sensor for isoniazid detection, Analyst 137 (2012) 3644–3652.
[18] M.F. Bergamini, D.P. Santos, M.V.B. Zanoni, Determination of isoniazid in human urine using screen-printed carbon electrode modified with poly-l-histidine, Bioelectrochemistry 77 (2010) 133–138.
[19] X.J. Si, L. Jiang, X.Y. Wang, et al., Determination of isoniazid content via cysteic acid/graphene modified glassy carbon electrode, Anal. Methods 7 (2015) 793–798.
[20] Z. Zhang, S. Zhang, L. He, et al., Feasible electrochemical biosensor based on plasma polymerization-assisted composite of polyacrylic acid and hollow TiO_2 spheres for sensitively detecting lysozyme, Biosens. Bioelectron. 74 (2015) 384–390.
[21] S.A. Kumar, C.F. Tang, S.M. Chen, Electroanalytical determination of acetaminophen using nano-TiO_2/polymer coated electrode in the presence of dopamine, Talanta 76 (2008) 997–1005.
[22] H.F. Cui, W.W. Wu, M.M. Li, et al., A highly stable acetylcholinesterase biosensor based on chitosan-TiO_2-graphene nanocomposites for detection of organophosphate pesticides, Biosens. Bioelectron. 99 (2018) 223–229.
[23] H.F. Cui, K. Zhang, Y.F. Zhang, et al., Immobilization of glucose oxidase into a nanoporous TiO_2 film layered on metallophthalocyanine modified vertically-aligned carbon nanotubes for efficient direct electron transfer, Biosens. Bioelectron. 46 (2013) 113–118.
[24] H. Liu, W. Li, D.K. Shen, et al., Graphitic carbon conformal coating of mesoporous TiO_2 hollow spheres for high-performance lithium ion battery anodes, J. Am. Chem. Soc. 137 (2015) 13161–13166.
[25] A.H. Liu, M.D. Wei, I. Honma, et al., Biosensing properties of titanate-nanotube films: selective detection of dopamine in the presence of ascorbate and uric acid, Adv. Funct. Mater. 16 (2006) 371–376.
[26] C.H. Yang, W.X. Que, X.T. Yin, et al., Improved capacitance of nitrogen-doped delaminated two-dimensional titanium carbide by urea-assisted synthesis, Electrochim. Acta 225 (2017) 416–424.
[27] M.H. Naveen, K. Shim, M.S.A. Hossain, et al., Template free preparation of heteroatoms doped carbon spheres with trace Fe for efficient oxygen reduction reaction and supercapacitor, Adv. Energy Mater. 7 (2017), 1602002.
[28] J.N. Zhang, X.L. Zhang, Y.C. Zhou, et al., Nitrogen-doped hierarchical porous carbon nanowhisker ensembles on carbon nanofiber for high-performance supercapacitors, ACS Sustainable Chem. Eng. 2 (2014) 1525–1533.
[29] T.K. Zhao, J.K. Zhang, Z. Du, et al., Dopamine-derived N-doped carbon decorated titanium carbide composite for enhanced supercapacitive performance, Electrochim. Acta 254 (2017) 308–319.
[30] J. Zhang, Q. Xu, Z. Feng, et al., Importance of the relationship between surface phases and photocatalytic activity of TiO_2, Angew. Chem. Int. Ed. Engl. 47 (2008) 1766–1769.
[31] S.X. Li, J. Chen, F.Y. Zheng, et al., Synthesis of the double-shell anatase-rutile TiO_2 hollow spheres with enhanced photocatalytic activity, Nanoscale 5 (2013) 12150–12155.
[32] R. Atchudan, T.N.J.I. Edison, S. Perumal, et al., *In situ* green synthesis of nitrogen-doped carbon dots for bioimaging and TiO_2 nanoparticles@ nitrogen-doped carbon composite for photocatalytic degradation of organic pollutants, J. Alloys Compd. 766 (2018) 12–24.
[33] W.W. Ji, Y.M. Mei, M. Yang, et al., The core-shell mesoporous titanium dioxide with *in situ* nitrogen doped carbon as the anode for high performance lithium-ion battery, J. Alloys Compd. 806 (2019) 946–952.
[34] R. Atchudan, N. Muthuchamy, T.N.J.I. Edison, et al., An ultrasensitive photoelectrochemical biosensor for glucose based on bio-derived nitrogen-doped carbon sheets wrapped titanium dioxide nanoparticles, Biosens. Bioelectron. 126 (2019) 160–169.
[35] Y. Zhang, C.W. Wang, H.H. Hou, et al., Nitrogen doped/carbon tuning yolk-like TiO_2 and its remarkable impact on sodium storage performances, Adv. Energy Mater. 7 (2017), 1600173.
[36] A.M. Abdullah, N.J. Al-Thani, K. Tawbi, et al., Carbon/nitrogen-doped TiO_2: New synthesis route, characterization and application for phenol degradation, Arab. J. Chem. 9 (2016) 229–237.
[37] S.X. Li, J.B. Cai, X.Q. Wu, et al., Fabrication of positively and negatively charged, double-shelled, nanostructured hollow spheres for photodegradation of cationic and anionic aromatic pollutants under sunlight irradiation, Appl. Catal. B Environ. 160–161 (2014) 279–285.
[38] W.G. Leng, M. Chen, S.X. Zhou, et al., Capillary force induced formation of monodisperse polystyrene/silica organic-inorganic hybrid hollow spheres, Langmuir 26 (2010) 14271–14275.
[39] G. Wu, K.L. More, C.M. Johnston, et al., High-performance electrocatalysts for oxygen reduction derived from polyaniline, iron, and cobalt, Science 332 (2011) 443–447.
[40] X.H. Kang, J. Wang, H. Wu, et al., A graphene-based electrochemical sensor for sensitive detection of paracetamol, Talanta 81 (2010) 754–759.
[41] A. Mao, H.B. Li, D.Q. Jin, et al., Fabrication of electrochemical sensor for paracetamol based on multi-walled carbon nanotubes and chitosan-copper complex by self-assembly technique, Talanta 144 (2015) 252–257.
[42] R. Liu, X.B. Zeng, J.C. Liu, et al., A glassy carbon electrode modified with an amphiphilic, electroactive and photosensitive polymer and with multi-walled carbon nanotubes for simultaneous determination of dopamine and paracetamol, Microchim. Acta 183 (2016) 1543–1551.
[43] Z.A. Alothman, N. Bukhari, S.M. Wabaidur, et al., Simultaneous electrochemical determination of dopamine and acetaminophen using multiwall carbon nanotubes modified glassy carbon electrode, Sens. Actuators B Chem. 146 (2010) 314–320.
[44] P. Chandra, N.X. Son, H.B. Noh, et al., Investigation on the downregulation of dopamine by acetaminophen administration based on their simultaneous determination in urine, Biosens. Bioelectron. 39 (2013) 139–144.
[45] B. Habibi, M. Jahanbakhshi, M.H. Pournaghi-Azar, Simultaneous determination of acetaminophen and dopamine using SWCNT modified carbon-ceramic electrode by differential pulse voltammetry, Electrochim. Acta 56 (2011) 2888–2894.
[46] N.T.T. Tu, P.C. Sy, T.V. Thien, et al., Microwave-assisted synthesis and simultaneous electrochemical determination of dopamine and paracetamol using ZIF-67-modified electrode, J. Mater. Sci. 54 (2019) 11654–11670.

[47] B. D Liu, X.Q. Ouyang, Y.P. Ding, et al., Electrochemical preparation of nickel and copper oxides-decorated graphene composite for simultaneous determination of dopamine, acetaminophen and tryptophan, Talanta 146 (2016) 114–121.
[48] L. Fu, K. Xie, Y. Zheng, et al., Graphene ink film based electrochemical detector for paracetamol analysis, Electronics 7 (2018), 15.
[49] Y. Kumar, P. Pramanik, D.K. Das, Electrochemical detection of paracetamol and dopamine molecules using nano-particles of cobalt ferrite and manganese ferrite modified with graphite, Heliyon 5 (2019), e02031.
[50] S.X. Li, L.X. Lin, F.Y. Zheng, et al., Metal bioavailability and risk assessment from edible brown alga Laminaria japonica, using biomimetic digestion and absorption system and determination by ICP-MS, J. Agric. Food Chem. 59 (2011) 822–828.
[51] L.X. Lin, F.Y. Zheng, H.F. Zhou, et al., Biomimetic gastrointestinal tract functions for metal absorption assessment in edible plants: Comparison to *in vivo* absorption, J. Agric. Food Chem. 65 (2017) 6282–6287.